Final Technical Report, May 2002
3-D MAPPING OF ACTIVE FAULTS IN SOUTHERN CALIFORNIA: EASTERN VENTURA BASIN AND SAN GORGONIO PASS—SAN BERNARDINO REGIONS.

NEHRP Award #01HQGR0028

John Suppe
Department of Geosciences
Princeton University
Princeton, NJ 08544
609-258-4119 (phone), 609-258-1274 (fax)
suppe@princeton.edu

Element I 50%, Element III 50%

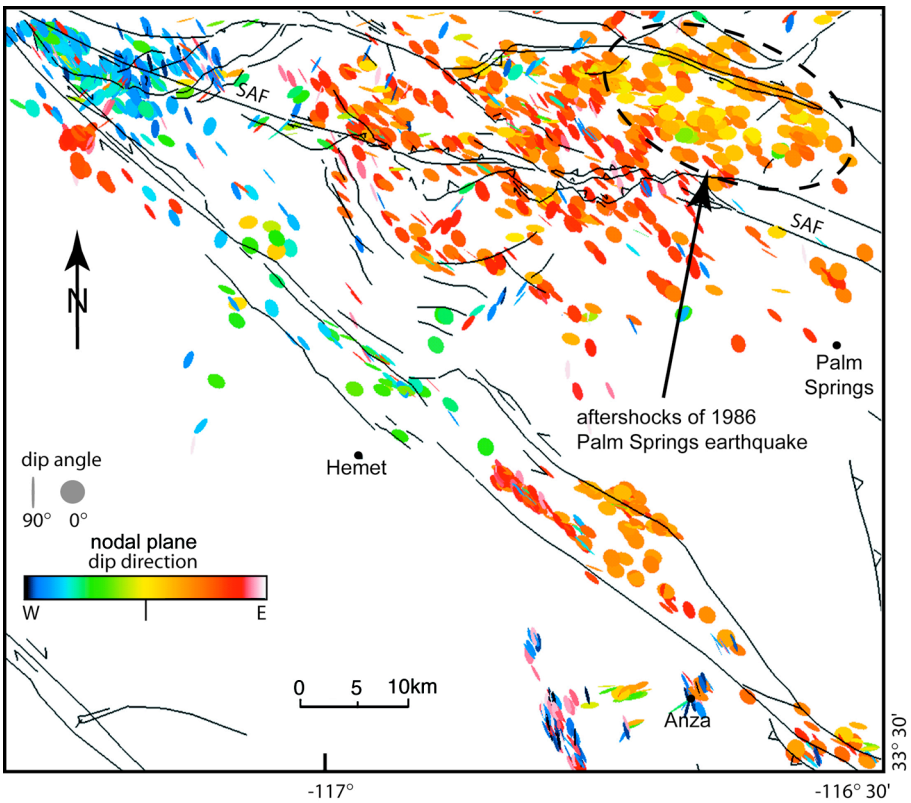

"Research supported by the U.S. Geological Survey (USGS), Department of the Interior, under USGS award number 01-HQ-GR-0028. The views and conclusions contained in this document are those of the authors and should not be interpreted as necessarily representing the official policies, either expressed or implied, of the U.S. Government."

This report is available online at http://geoweb.princeton.edu/people/grads/carena/SGPreport.pdf

TABLE OF CONTENTS

NEHRP Award #01HQGR0028

3-D MAPPING OF ACTIVE FAULTS IN SOUTHERN CALIFORNIA: EASTERN VENTURA BASIN AND SAN GORGONIO PASS—SAN BERNARDINO REGIONS.

John Suppe
Department of Geosciences
Princeton University
Princeton, NJ 08544
609-258-4119 (phone), 609-258-1274 (fax)
suppe@princeton.edu

TECHNICAL ABSTRACT

We mapped over 70 faults in the San Gorgonio Pass-San Bernardino Mountains region using the catalog of 43,500 relocated 1975-1998 earthquakes of Richards-Dinger and Shearer (2000). A clustering algorithm was applied to the relocated earthquakes in order to obtain tighter earthquake clouds and thus better-defined fault surfaces. The earthquakes were then imported into Gocad, a 3D modeling software that allowed us to separate earthquakes into coplanar clusters associated with different faults and fault strands and to fit optimized surfaces to them. We also used the catalog of 13,000 focal mechanisms of Hauksson (2000) to confirm the nature of the mapped faults. Two locations are particularly interesting. Near Anza, the major San Jacinto strike-slip fault zone is offset by low-angle faults at several locations, in what appear to be stable fault intersections. At San Gorgonio Pass, our findings suggest that the existence of a through-going vertical or near-vertical San Andreas fault is highly unlikely. In order to pass through this region, the San Andreas fault must rotate to much shallower dips, or lose its continuity at depths between 0 and 15 km, with most of the slip in this depth range transferred to the faults that form the complex network in this area.

NEHRP Award #01HQGR0028

3-D MAPPING OF ACTIVE FAULTS IN SOUTHERN CALIFORNIA: EASTERN VENTURA BASIN AND SAN GORGONIO PASS—SAN BERNARDINO REGIONS.

John Suppe
Department of Geosciences
Princeton University
Princeton, NJ 08544
609-258-4119 (phone), 609-258-1274 (fax)
suppe@princeton.edu

NON-TECHNICAL SUMMARY

We imaged and mapped in 3-D over 70 active faults in the San Gorgonio Pass – San Bernardino Mountains region using earthquake locations and focal mechanisms. The majority of these faults are previously unknown or unnamed. The 3-D fault maps better define the active structure of this complex region marked by profound uncertainties over the fundamental structural framework, including the subsurface continuity and geometry of the first-order San Andreas and San Jacinto faults, as well as the existence and role of major blind faults, some of which are as large as the rupture area of the Northridge earthquake.

1.0 INTRODUCTION

Small earthquakes are spatially-specific data for imaging subsurface structures, but so far they have not been fully exploited as such, although some recent work has illustrated their potential. For example *Seeber and Armbruster* [1995a, 1995b] have shown that blind faults in the San Gorgonio Pass and Northridge areas can be identified by viewing large sets of focal mechanisms in 3-D and *Shaw and Shearer* [1999] have combined relocated aftershock data with reflection profiling to identify the source of the Whittier Narrows earthquake. In recent years we have experimented—in part through undergraduate thesis projects—with using aftershocks from large earthquakes to model faults by fitting surfaces in 3-D to earthquake clouds [*Shaw et al*. 1994, *Brankman 1995, Van Dusen 1997;Carena and Suppe 1999a, 1999b, Carena 1999, Carena et al., 2002*]. We developed a series of techniques, testing them with the Landers, Loma Prieta and Northridge aftershocks, as well as on background seismicity. We are now able to create structurally reasonable fault surfaces by selecting and fitting 3-D surfaces to earthquake clusters within the powerful *Gocad* 3-D Earth modeling software environment.

This is the first part of a two-part study: here we focus on the region centered on San Gorgonio Pass, from the San Bernardino Mountains to the north, to Anza to the south (figure 1). The Ventura basin is part of a continuation project currently under way, and some results are included in the bibliography of this report.

1.1 OBJECTIVES

The vast numbers of routinely recorded small earthquakes that constitute the bulk of regional catalogues are a valuable but under-utilized resource for earthquake hazard studies. We demonstrate that these small earthquakes (combined with surface and subsurface geologic data) can be routinely used to construct 3-D maps (digital 3-D surfaces) of many active faults. To do this is not simply a matter of 3-D visualization of the earthquake 'clouds'; it requires robust techniques for working in 3-D to obtain optimized fits of structurally-reasonable surfaces to the data (quasi-threaded surfaces constrained by hypocentral locations with errors, focal mechanisms, and geologic constraints). In the San Gorgonio Pass area we were able to identify significant previously unrecognized blind faults, and map known faults that break the surface in greater 3-D detail, including potential segment boundaries. These digital maps will be made widely available in convenient formats (for example, through the *SCEC Community Fault Model*, currently under development) to provide a basis for improved geographically specific earthquake-hazard scenarios and better geodetic and seismic source modeling. These 3-D surfaces also provide for improved 3-D visualization and public communication of the seismic risks in southern California (for example as "fly-through" 3-D visualizations released to the news media and on the web). Fundamentally, however, we seek to provide detailed 3-D maps of the complex networks of active faults in key areas of southern California.

1.2 METHODS

In general, the basic data we use to develop 3-D models of fault surfaces are earthquake hypocenter locations. For a complex fault with an area of about 500 km^2, the optimal number of data points for imaging the surface at high resolution is around 5,000. Nevertheless, this number can be much lower when the fault geometry is very simple, earthquakes are very well located or when additional information like focal mechanisms, surface ruptures, well data, etc are available. Useful but lower resolution results can be obtained with as few as 10-100 earthquakes, combined with other data.

For this project, we downloaded *Richards-Dinger and Shearer* [2000] hypocenter location data from the SCEC database (figure 2a). This catalog contains 43,500 events in our study area recorded in the period 1975-1998 and relocated. These hypocenter locations were then clustered using the method developed by *Jones and Stewart* [1996] and by *Nicholson et al.* [2000] (figure 2b). Clustering makes the subsequent process of selecting subsets of earthquakes much easier, and can enlighten details of the fault surface otherwise masked by scattering of the hypocenters (figure 3). This method can be applied whenever (1) the events were recorded by a local network; (2) information about location errors is preserved in the catalog or is recoverable in some way; and (3) the earthquake clouds are dense enough that there is overlap between earthquake error ellipsoids.

The hypocenter locations are then imported into *Gocad*, which among other things allows viewing them in 3-D, fitting 3-D surfaces to sets of points, and obtaining fitting statistics. Stereo glasses enable us to look at the clusters of events from every angle in 3-D and separate clusters associated with different faults. Surface breaks that could be associated with faults at depth are also imported at this stage. Surface breaks constrain the position of the top of the fault and may disclose a change in fault dip that could have gone undetected, since there are generally only a few events at very shallow depths. They can also provide information regarding possible fault splays near the Earth's surface or other shallow faults.

Focal mechanisms can be used to further constrain the fault geometry; they are particularly useful when there is a low density of hypocenters. For this study we were able to download 13,000 focal mechanisms made available by *Hauksson* [2000] on the SCEC database. As demonstrated by *Seeber and Armbruster* [1995b], focal mechanisms can be used to identify complex fault interactions even in areas of sparse seismicity. The comparison between earthquake hypocenter distribution and focal mechanisms in 3D allowed us to [1] distinguish between principal and auxiliary nodal planes, [2] identify and map faults, which have only a few events associated with them, [3] determine the current slip direction on several faults. For the San Bernardino Mountains area, we also imported into Gocad the cross-sections of *Spotila and Sieh* [2000], which give us constraints on several faults that did not produce much seismicity over the last 20 years, and are thus invisible in the earthquake data alone.

The next step is to generate fault surfaces from the identified clusters and the integrated

additional data (figure 4). A cloud of earthquakes can theoretically be fit with a plane using a least squares inversion. But such a simple fault model is not relevant for the purpose of building structurally realistic surfaces. In many cases real faults have a rather complex geometry and may be highly three-dimensional. In the best case, faults show changes in dip and/or strike. A least squares fit gives the average strike and slip of the fault, but it will miss any step, bend, splay, or changes in dip and strike. Not only steps and bends are often the starting point of major earthquakes [*Shaw et al*., 1994], but also any change in the fault orientation is a potential source of either folds or other faults [e.g. *Suppe* 1983, *Shaw and Suppe* 1996, *Shaw and Shearer* 1999]. Therefore we use irregular triangulated surfaces as the basis of fitting the hypocentral locations. If any other kinds of data are available, they can be used to constrain a fault surface even further, either during the initial fitting or during smoothing, which is the next step in the process. The surface is smoothed with the *Gocad* DSI algorithm [*Mallet*, 1997] (figure 4). The smoothing will preserve any major feature of the surface, like changes in strike and dip, bends, steps, etc., but will smooth out all those minor "bumps" created by the fitting procedure that in most cases are the result of earthquake scattering due to original location errors not filtered out by relocation procedures. During the smoothing procedure "control nodes" can be set to keep the position of specific nodes on the triangulated surface fixed: surface breaks are a good example of data points that can be used as control nodes. The final product is a smooth surface which preserves all the major geometric features already existing in the original earthquake cloud, but where the minor irregularities due to scattering have been eliminated.

The resolution of our fault models does of course depend on the original accuracy in the hypocenter locations [*Carena and Suppe*, 2002]. We cannot resolve any structures smaller than the average hypocenter location errors (about 0.6 km horizontal error, 1.8 km vertical error for our present study), as any structures below this size could very well be artifacts of the clustering process. This fact has implications for the definition of fault "plane" versus fault "zone": the distinction between the two is contingent upon the desired level of detail. For convenience, we call our models "fault surfaces", as most of them are defined by a band of earthquakes whose width is close to our resolution limit, and we cannot resolve any finer structures (like thinly spaced, parallel faults) within these bands. If the fault in question is indeed a fault zone, our surface will simply represent the middle of the illuminated fault zone, which corresponds to the maximum earthquake density.

2.0 TECTONIC SETTING

Two major converging fault zones, the San Andreas fault zone and the San Jacinto fault zone, dominate the area between the San Bernardino Mountains to the north and Anza to the south (figure 1). The much younger San Jacinto fault zone consist of many en echelon fault strands, while most of the San Andreas fault zone is more or less a continuous fault [*Morton and Matti*, 1993]. However, the 15 km left-step of the San Andreas at San Gorgonio Pass interrupts this continuity and gives rise to surface geometries far more complicated than those of the San Jacinto [*Matti et al*., 1985].

The San Gorgonio-San Bernardino region is indeed very complex, with the San Andreas fault splitting into several strands, and an extremely high level of seismicity on many faults except the San Andreas itself [*Petersen and Wesnousky* 1994, and figures 1, 2]. In fact, there is no trace of the San Andreas at shallow levels in this area [*Allen* 1957, *Matti et al*. 1992], and some authors consider it unlikely for the fault to be continuous here even at depth [*Magistrale and Sanders* 1996]. Besides the San Andreas, other faults capable of producing damaging earthquakes exist in this area [e.g. *Spotila and Sieh*, 2000].

3.0 RESULTS

The work of *Seeber and Armbruster* [1995b] shows that the complex fault interactions in this region can be successfully imaged in 3-D by plotting earthquake focal mechanisms. We have carried this work further, separating the different faults and fault strands and fitting 3-D surfaces to them. Starting from the hypocenter locations of *Richards-Dinger and Shearer* [2000] (figure 2a), and from the focal mechanisms of *Hauksson* [2000] (figures 6, 7), we modeled 72 faults and fault segments from the collapsed earthquakes alone (figure 5b). Moreover, we added several other major faults to our 3D fault model (figure 8a), based on surface rupture maps and published papers (*Jennings*, 1994; *Spotila and Sieh,* 2000; *Morton and Matti,* 1993). Several of the blind faults we imaged from the earthquakes have sizes comparable to the 1994 Northridge earthquake rupture area.

Our study shows that knowing the position and geometry of smaller faults with relatively low slip rates can be very helpful in constraining the location and geometry of large strike-slip faults in areas where the latter are aseismic. The geometry of the strike-slip fault must be compatible with the geometry, location, and slip direction on the smaller faults. Two subregions are particularly interesting as far as fault interactions are concerned: the area NE of Anza (box A, figure 5b), and the area surrounding the San Gorgonio Pass fault trace (box B, figure 5b).

3.1 *Geometrical constraints*

When a sub-vertical fault and a low angle fault intersect, their intersection line can be either horizontal or oblique (dipping) (figure 9). In our study area, we have several examples of sub-vertical, fast-slipping, right-lateral strike-slip faults (San Andreas, most of the San Jacinto strands, Petersen *and Wesnousky*, 1994) and low-angle faults with a reverse slip component (for example, the San Gorgonio thrust system), so we will examine intersections between these kinds of faults.
1) If the intersection is horizontal, i.e. parallel to the strike of both faults involved, slip on the strike-slip fault will offset the low-angle fault, but not interrupt the continuity of its rupture plane (figure 9a). Under these conditions, the low-angle fault can still have dip-slip events without having to create an entirely new rupture plane. There is one exception: continuity of the low-angle plane will be interrupted if the strike-slip fault has a significant dip-slip component.

2) If the intersection is oblique however, slip on the strike-slip fault will interrupt the continuity of the low-angle plane, making future reverse slip events on the latter much less likely (figure 9b). The only exception, in which continuity of the low-angle plane will not be interrupted, is if the slip direction on the strike-slip fault is parallel to the line of intersection between the two faults, which can require a substantial amount of dip-slip on the sub-vertical fault.

3.2 *Anza region*

We observe the major San Jacinto strike-slip fault zone to be offset by low-angle faults at several locations near Anza. The low-angle faults occur at depths between 10 and 20 km (figures 5, 10). Focal mechanisms on the low-angle faults indicate generally oblique right-lateral/reverse slip, with some mechanisms on the southernmost low-angle fault showing nearly pure strike-slip. The strong right-lateral slip component of the thrusts means that they will not offset the San Jacinto fault much during a single slip event, as a large part of the offset will simply be parallel to the strike of the San Jacinto itself.
The intersections between the San Jacinto and the low-angle faults vary from horizontal (figure 5) to about 10° plunge to the NW. *Petersen and Wesnousky* (1994) point out that in some sections (including Anza) the San Jacinto could have up to 10% reverse slip component (which translates roughly into an average slip vector 6° from the horizontal), and a similar component is visible in the focal mechanisms as well (figure 10a). As the reverse slip vector component on the San Jacinto is close in orientation to some of the most oblique fault intersections, and in any case it is not far from horizontal, slip on the San Jacinto should not create a discontinuity in the thrusts large enough to shut them down. The fact that both the low-angle faults and the San Jacinto segments appear to be active and well-developed seems to confirm that their intersections are relatively stable. This stable relationship observed at Anza serves as a useful model for the San Andreas fault at San Gorgonio Pass.

3.3 *San Gorgonio Pass*

Here the San Andreas fault does not have a clear surface trace and it is aseismic. We first obtained 3D models for several faults in this area (figures 5-8), and then verified if there are solutions for the 3D geometry of a steeply dipping San Andreas that would allow it to pass through this region, at least at depths greater than 2-3 km below sea level. In fact, the absence of a clear San Andreas trace above the San Gorgonio Pass thrust system is a strong indicator that the thrust can prevent the development of a well-localized San Andreas rupture at shallow depth, but it does not mean that a continuous sub-vertical San Andreas cannot exist below the thrusts themselves. Also, before it disappears, the San Andreas trace curves south when it encounters the western and eastern ends of the San Gorgonio Pass fault zone, suggesting that the bending could be a consequence of reverse slip on this thrust system.
We obtained a preliminary geometry for the San Gorgonio thrust (*SGPT* in figures 11 and 12) from its surface trace and the assumption that its orientation is similar to the one

of the segments that produced many aftershocks in the M_L 5.6, 1986, North Palm Springs earthquake (*SGPTb* in figures 11, 12, 13, considered part of the San Gorgonio Pass thrust zone by *Seeber and Armbruster*, 1995b). Another condition we imposed is for the intersection between the *SGPT*/*SGPTb* and the San Andreas to be horizontal, because otherwise major slip events on the San Andreas would shut down the SGPT system. Unlike the San Jacinto fault, the San Andreas appears to be pure strike-slip everywhere (*Petersen and Wesnousky*, 1994), and under such conditions the stability of an oblique intersection is not possible. With a horizontal intersection, the San Andreas fault can still be continuous at depth, and both faults can slip without interfering with each other. The illuminated part of the *SGPTb* satisfies this condition (figures 11, 12b). Changing the dip of the *SGPT* will not change this result, as long as the strike remains the same. Thus the presence of the San Gorgonio Pass fault system is not the limiting factor for the existence of a deep, continuous, sub-vertical San Andreas.

However, there are other faults in this area that must be taken into consideration. Of all the faults shown in figure 12b, only *F3* is positioned in such a way that an "interpolated" sub-vertical San Andreas would crosscut it in an unstable geometry (non-horizontal intersection). *F3* is very well constrained by earthquakes (500 hypocenter locations distributed in a band barely 2 km wide at its widest point, 60 consistent focal mechanisms, with prevalent right-lateral strike-slip), and the intersection with a deep San Andreas would be strongly oblique, cutting *F3* in half. *F3* does not show any offset at our current resolution (about 600 m for horizontal offsets). There are three different scenarios that do not involve visible offset of *F3* as a consequence:

(a) The San Andreas fault (SAF) is not continuous at San Gorgonio Pass between 3 and 15 km depth, the deepest point of possible intersection between San Andreas and *F3*. This leaves only 2-3 km to the base of the seismicity in this region (figures 8b, 12a). *F3* and other faults sub-parallel to it (*F1, F2* and several others) could be taking up part of the San Andreas slip in the upper 15 km of the crust. The San Gorgonio Pass thrust faults also have a significant component of right-lateral strike slip, as shown by the focal mechanisms of *Hauksson* [2000] and as indicated by the right offsets on the thrust traces west of San Gorgonio Pass.

(b) The deep south SAF (seSAF, figure 11) does not connect in a straight line to the deep north SAF (nSAF), but follows a more complex path. The simplest solution in this case is for the deep south SAF to "skirt" *F3* on its eastern side (possibly following at depth the trace of the surface Mill Creek or the Mission Creek faults), and then turn west, parallel to the strike of the *SGPT* surface trace. Any path south of *F3* would have to be even more complex, or the San Andreas would have to be far from vertical. The latter hypothesis calls for dips and fault location that basically coincide with those of the *SGPT* system.

(c) *F3* (and, likely, all the other sub-parallel structures, including *F1* and *F2*) is very young. Probable offsets on the Yucaipa segment of the San Andreas (*Petersen and Wesnousky*, 1994) vary between 300 m (14,000-20,000 yrs) and 1040 m (69,000-90,000 yrs). Offsets in the upper part of this range should already be visible at our resolution, therefore *F3* would have to be younger than about 60,000 years.

F3 does not seem at first to have any specific surface expression. However the strikes of *F3, F2, F*1, and several other nearby faults are close to that of the right-lateral offsets on the thrust traces west of San Gorgonio Pass. In fact, *F3, F2* and *F1* updip projections either coincide or fall within 500 m of three such offsets (figure 14).

Thus mapping the seismically illuminated faults places severe 3D constraints on the location, geometry, and possible segmentation of the aseismic San Andreas fault. We believe that by combining our fault models with paleoseismic studies it should be possible to determine which one of the plausible scenarios is the most likely at San Gorgonio Pass.

4.0 CONCLUSIONS

We were able to map over 70 faults from seismicity in the region between the San Bernardino Mountains to the north and Anza to the south. Near Anza, the major San Jacinto strike-slip fault zone is offset by low-angle faults at several locations, in what appear to be stable fault intersections. At San Gorgonio Pass, our findings suggest that the existence of a through-going vertical or near-vertical San Andreas fault is highly unlikely. In order to pass through this region, the San Andreas fault must either rotate to much shallower dips, or lose its continuity at depths between 0 and 15 km, with most of the slip in this depth range transferred to the faults that form the complex network at San Gorgonio Pass.

5.0 ACKNOWLEDGMENTS

Research work on the San Gorgonio Pass and Ventura basin faults is funded by the U.S.G.S. National Earthquake Hazards Reduction Program, awards number 01HQGR0028 and 02HQGR0033.
We thank Dr. Honn Kao (Academia Sinica, Taiwan) for help in clustering the earthquakes.

6.0 BIBLIOGRAPHY

Publications resulting from this project:

Carena, S., Suppe, J., 2002. - 3-D Imaging of Active Structures Using Earthquake Aftershocks: the Northridge Thrust, California. *J. Struct. Geol.*, **24**, 887-904.

S. Carena, J. Suppe, 2000 - Imaging Faults in 3-D with Microearthquakes. Proceedings of the Annual Meeting of the Geological Society in Taiwan (March 30-31, 2000). Abstract.

7.0 REFERENCES CITED

Allen, C.R., 1957. - San Andreas fault zone in San Gorgonio Pass, southern California. *Geol. Soc. Am. Bull.*, **68**, 315-350.

Brankman, C.M., 1995. - Relative relocation of aftershocks of the 1994 Northridge California Earthquake. BS thesis Princeton University Dept.Geol. & Geophys.Sci./Geol.Eng.Prog.

Carena, S., 1999. - 3-D Imaging of Faults Using Aftershocks of Large Earthquakes. EUG 10. J. Conf. Abs. **4**, 455 (abstract).

Carena, S. and J. Suppe, 1999a. - The Importance of Small Earthquakes and Good Locations in the Hunt for Blind Faults: the Example of Northridge. Eos, Transactions, American Geophysical Union. **80**; 46, Suppl., 644 (abstract).

Carena, S. and J. Suppe, 1999b. - 3-D Structure of the Northridge area. Abstracts with Programs, Geological Society of America. (abstract).

Carena, S., Suppe, J., 2002. - 3-D Imaging of Active Structures Using Earthquake Aftershocks: the Northridge Thrust, California. *J. Struct. Geol.*, **24**, 887-904.

Carena, S., Suppe, J., Kao, H., 2002 - The Active Detachment of Taiwan Illuminated by Small Earthquakes and its Control of First-Order Topography**.** *Submitted to Geology.*

Hauksson, E., 2000. – Crustal Structure and Seismicity Distribution Adjacent to the Pacific and North America Plate Boundary in Southern California. *J. Geophys. Res.* **105**, 13875-13903.

Jennings, C.W., 1994. - Fault Activity Map of California and Adjacent Areas with Location and Ages of Recent Volcanic Eruptions. California Geologic Data Map Series, Map No. 6. California Division of Mines and Geology.

Jones, R.H, Stuart, R.C., 1997. - A method for determining significant structures in a cloud of earthquakes. *J.Geophys. Res.* **102**, 8245-8254.

Magistrale, H., Sanders, C., 1996. - Evidence from precise earthquake hypocenters for segmentation of the San Andreas fault in San Gorgonio Pass. *J. Geophys. Res.* **101**, 3031-3044.

Mallet, J.L., 1997. - Discrete modeling for natural objects. *Mathematical Geol.*, 29 (2), 199-219.

Matti, J.C., Morton, D.M., Cox, B.F., 1985. – Distribution and geologic relations of fault systems in the vicinity of the central Transverse Ranges, southern California. *USGS Open File Report* **85-365**, 27 pp., scale 1:250,000.

Matti, J.C., Morton, D.M., Cox, B.F., 1992. - The San Andreas fault system in the vicinity of the central Transverse Ranges province, southern California. *USGS Open File Report* **92-354**, 40 pp.

Morton, D.M., Matti, J.C., 1993 – Extension and contraction within an evolving divergent strike-slip fault complex: The San Andreas and San Jacinto fault zones at their convergence in southern California. *Geol. Soc. Am. Mem.*, **178**, 217-230.

Nicholson T., Sambridge M., Gudmundsson, O., 2000 - On entropy and clustering in earthquake hypocentre distributions. *J. Geophys. Int.*, **142**, 37-51.

Petersen, M.D., Wesnousky, S.G., 1994. - Fault Slip Rates and Earthquake Histories for Active Faults in Southern California. *Seismol. Soc. Am. Bull.*, **84** (5), 1608-1649.

Richards-Dinger, K., Shearer, P.M., 2000. – Earthquake Locations in Southern California Obtained Using Source Specific Station Terms. *J. Geophys. Res.* **105** (5), 10939-10960.

Seeber, N., Armbruster, J., 1995a. - Faults and stress from earthquakes in southern California. *Southern California Earthquake Center 1994 Annual Report*, (Southern California Earthquake Center, Los Angeles, CA), vol. II, pp. F37-F38.

Seeber, N., Armbruster, J., 1995b. - The San Andreas fault system through the Transverse Ranges as illuminated by earthquakes. *J. Geophys. Res.* **100**, 8285-8310.

Shaw, J.H., Bischke, R.E., Suppe, J., 1994. Relations between folding and faulting in the Loma Prieta epicentral zone: strike-slip fault-bend folding. In: Simpson, R.W. (Ed.), The Loma Prieta, California, earthquake of October 17, 1989; tectonic processes and models. *USGS Prof. Paper* **1550**, pp. F3-F21.

Shaw, J.H., Shearer, P.M., 1999. - An elusive blind-thrust fault beneath metropolitan Los Angeles. *Science* **283**, 1516-1518.

Shaw, J.H., Suppe, J., 1996. - Earthquake hazards of active blind-thrust faults under the central Los Angeles basin, California. *J. Geophys. Res.*, **101**, 8623-8642.

Spotila, J.A., Sieh, K., 2000. – Architecture of transpressional thrust faulting in the San Bernardino Mountains, southern California, from deformation on a deeply weathered surface. *Tectonics*, **19** (4), 589-615.

Suppe, J., 1983. - Geometry and kinematic of fault-bend folding. *Am. .J. Sci.* **283**, 684-721.

Van Dusen, A.B., 1997. - Determining three-dimensional fault shape from earthquake hypocenters; an assessment of GOCAD in modelling a fault surface with application to the June 28, 1992, Landers, California, earthquake. BA thesis Princeton University, Dept. Geosciences.

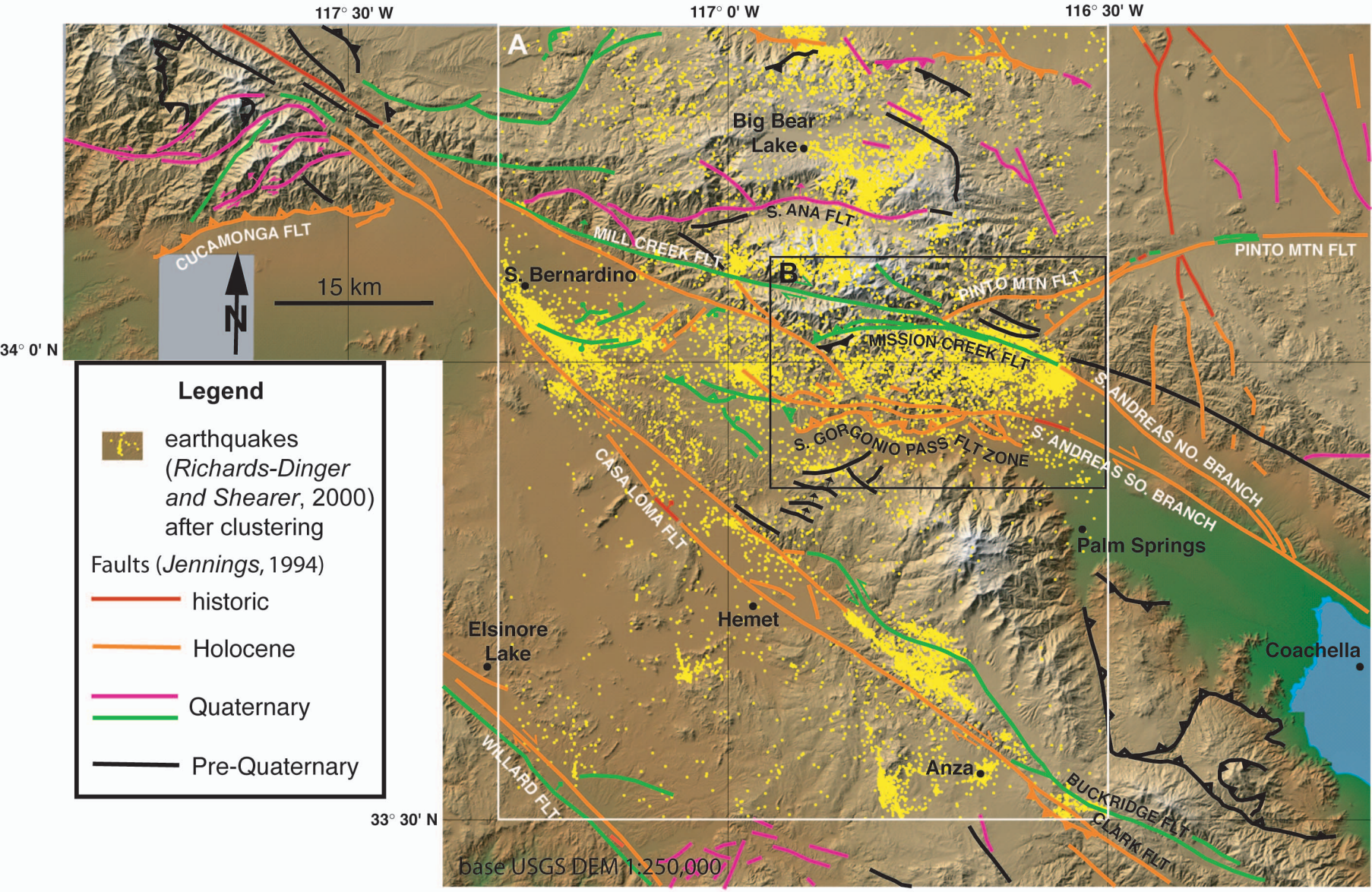

Figure 1. Location map and topography. Box A shows the location of figures 2, 5 and 8; box B shows the location of figure 11.

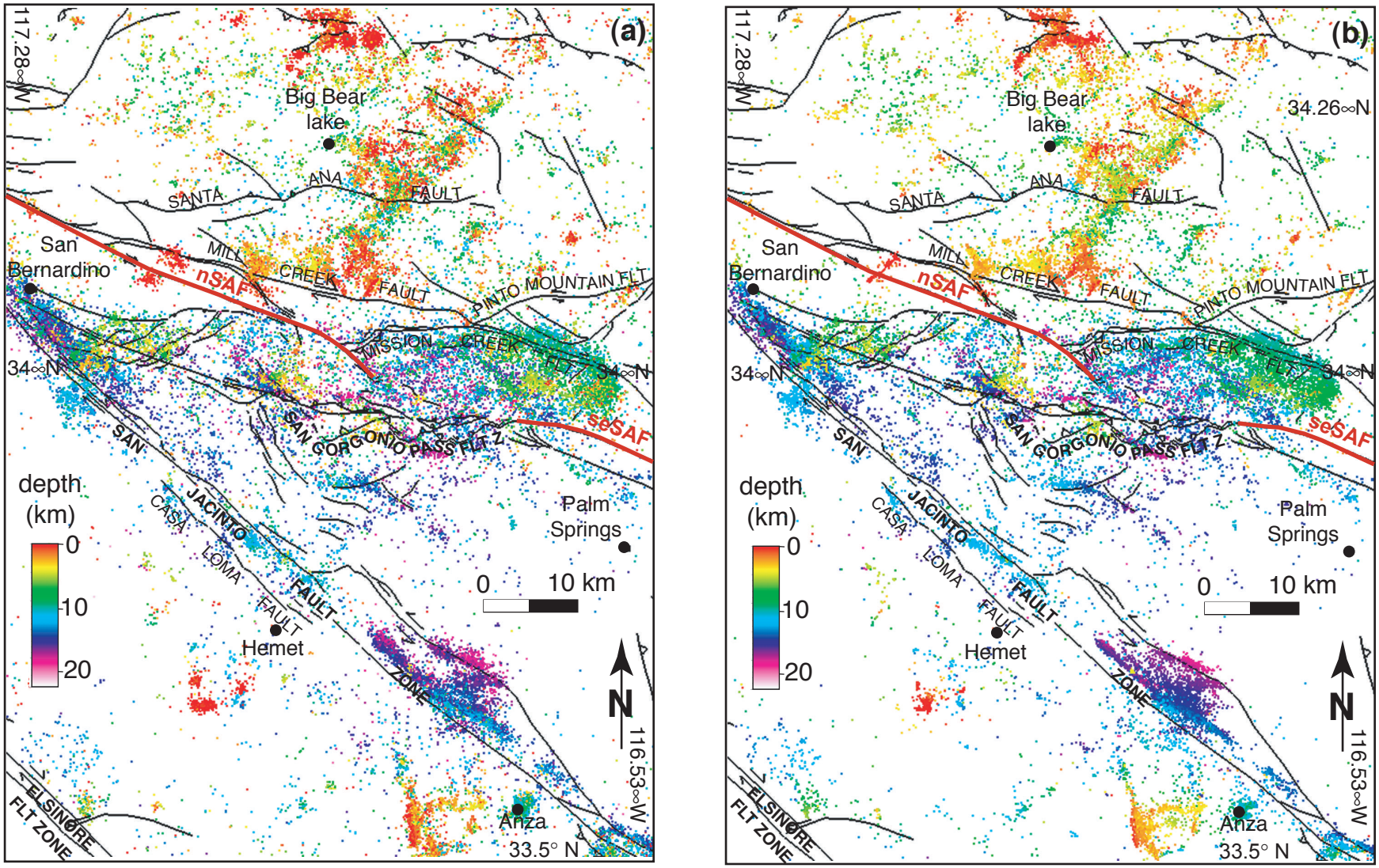

Figure 2. San Bernardino-San Gorgonio Pass area. Map showing 43,400 relocated events recorded between 1975 and 1998 [*Richards-Dinger and Shearer,* 2000] before (a) and after clustering (b). Fault traces are from *Jennings* [1994], and from *Matti and Morton* [1993]. nSAF = northwestern trace of the San Andreas fault, seSAF = southeastern trace of the San Andreas fault.

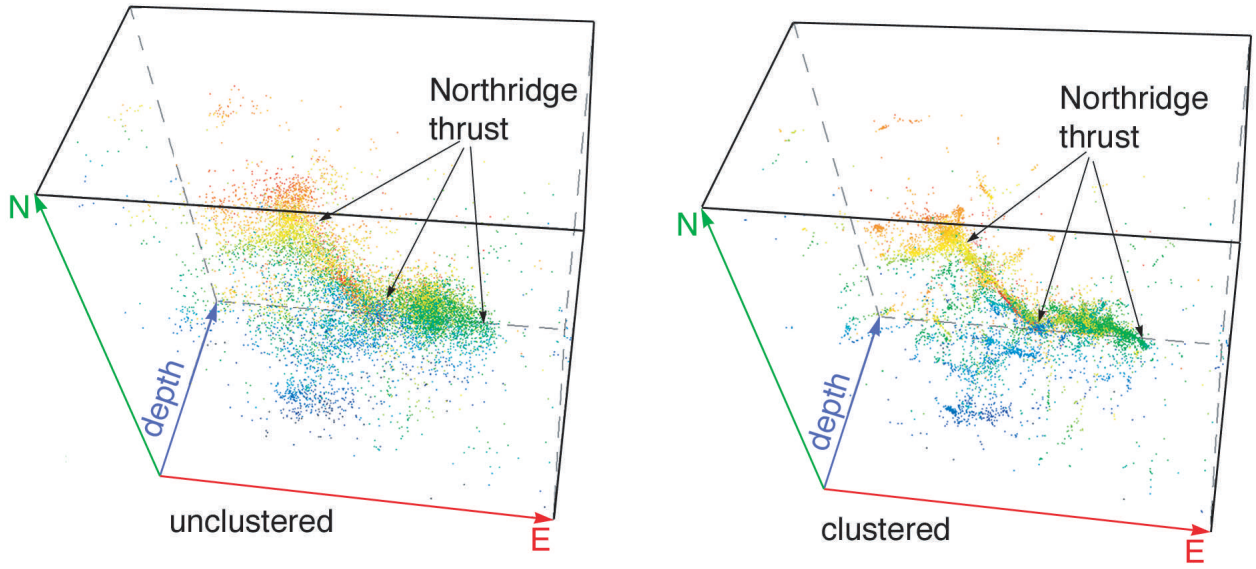

Figure 3. Example of earthquake hypocenters before (left) and after (right) clustering. The general distribution of earthquakes does not change, but the details become much sharper after clustering. This is a view of the 1994 Northridge earthquake aftershocks, looking downdip along the Northridge thrust. Color indicates depth, from 3 km (red) to 25 km (dark blue).

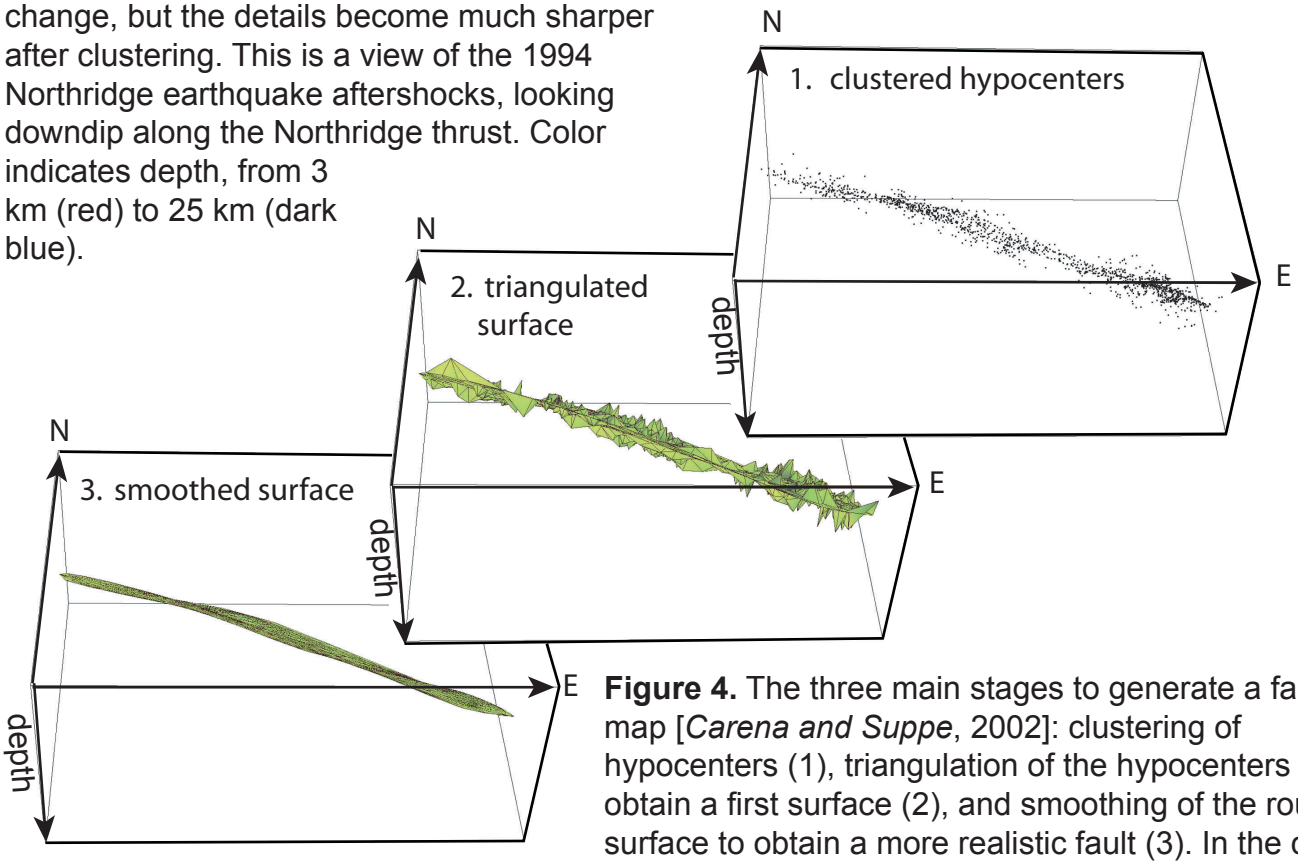

Figure 4. The three main stages to generate a fault map [*Carena and Suppe*, 2002]: clustering of hypocenters (1), triangulation of the hypocenters to obtain a first surface (2), and smoothing of the rough surface to obtain a more realistic fault (3). In the case when the earthquakes can be better interpreted with a fault zone of finite thickness, this surface corresponds to the location of the middle of the zone. In most instances, fault zone vs. fault surface depends on the scale of the problem and on the desired level of detail. The example used here is the fault labeled *SGPTb* in figure 11.

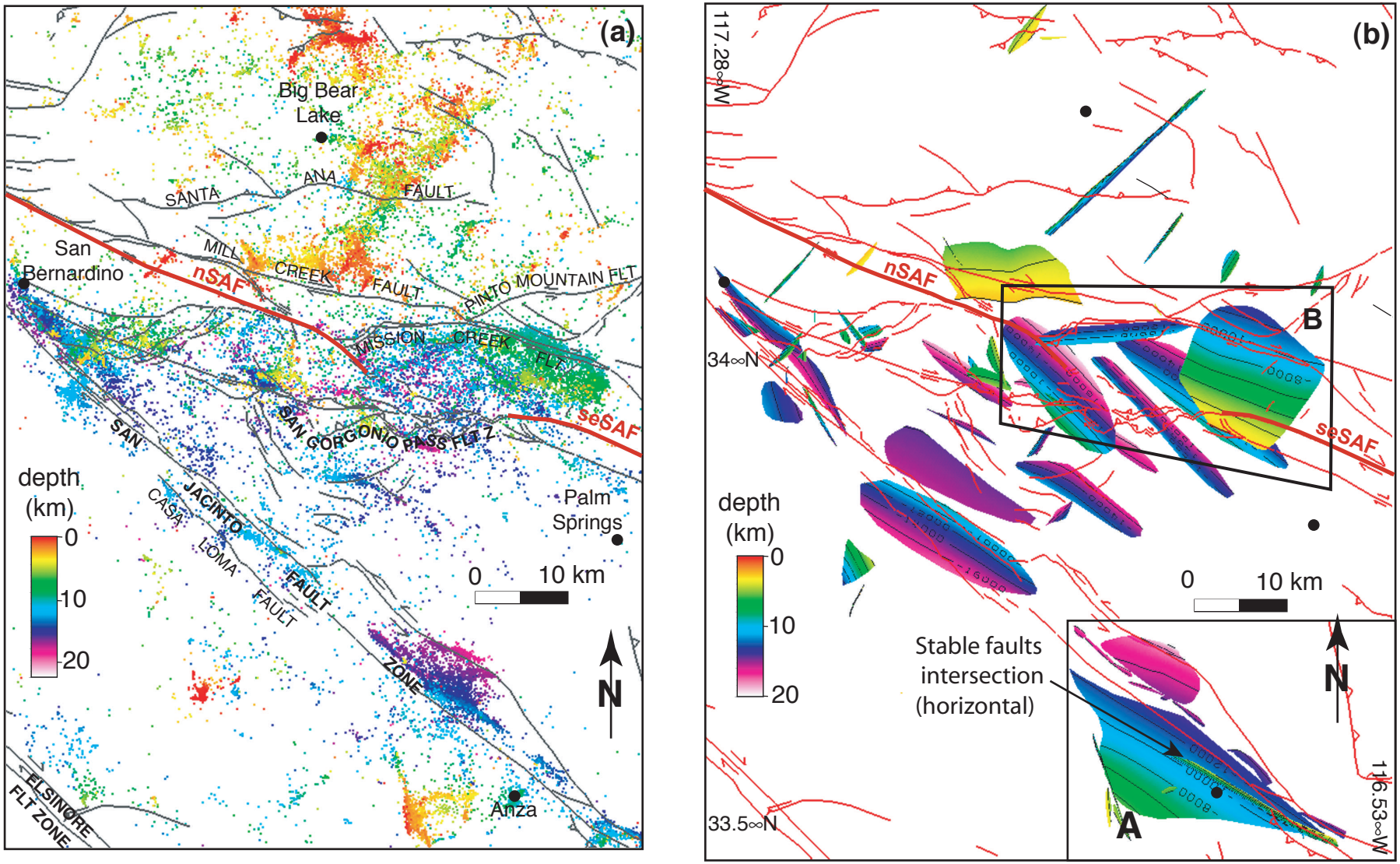

Figure 5. San Bernardino-San Gorgonio Pass area. Map showing 43,400 relocated events recorded between 1975 and 1998 [*Richards-Dinger and Shearer,* 2000] after clustering (a). Note how seismicity is consistently shallower north of the Mill Creek fault and deeper south of it. We used coplanar hypocenter clusters combined with the 13,000 nodal planes solutions of *Hauksson* [2000] to obtain the 72 fault models shown in (b). Box A in (b) indicates the location of figure 10, box B indicates the location of figure 12. Fault traces are from *Jennings* [1994], and from *Matti and Morton* [1993]. nSAF = northwestern trace of the San Andreas fault, seSAF = southeastern trace of the San Andreas fault.

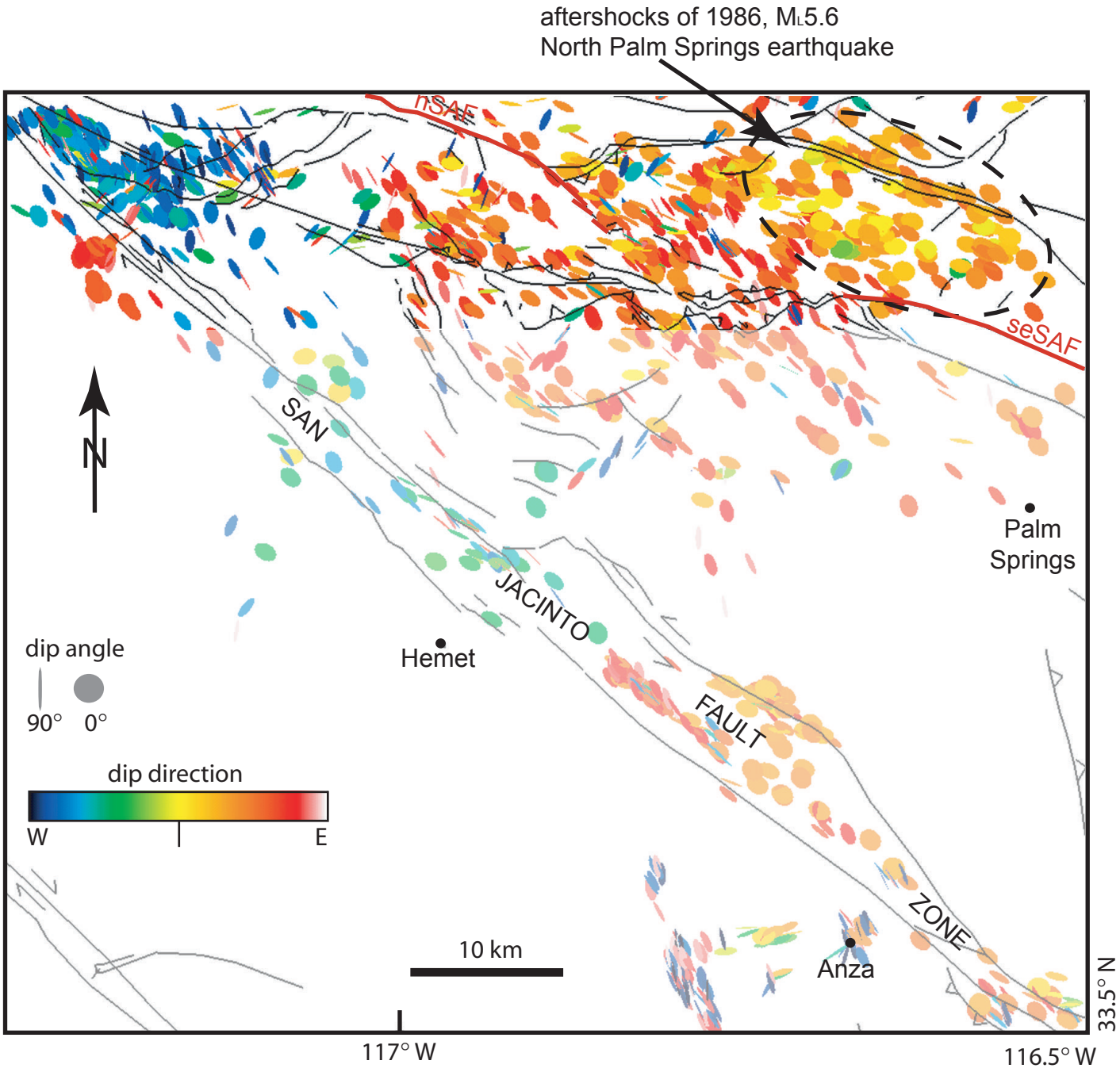

Figure 6. Map of 1539 selected nodal planes from Hauksson [2000]. Color indicates dip direction: in the San Gorgonio Pass area, nearly all planes dip to the NE. nSAF = NW branch of the San Andreas fault, seSAF = SE branch of the San Andreas fault.

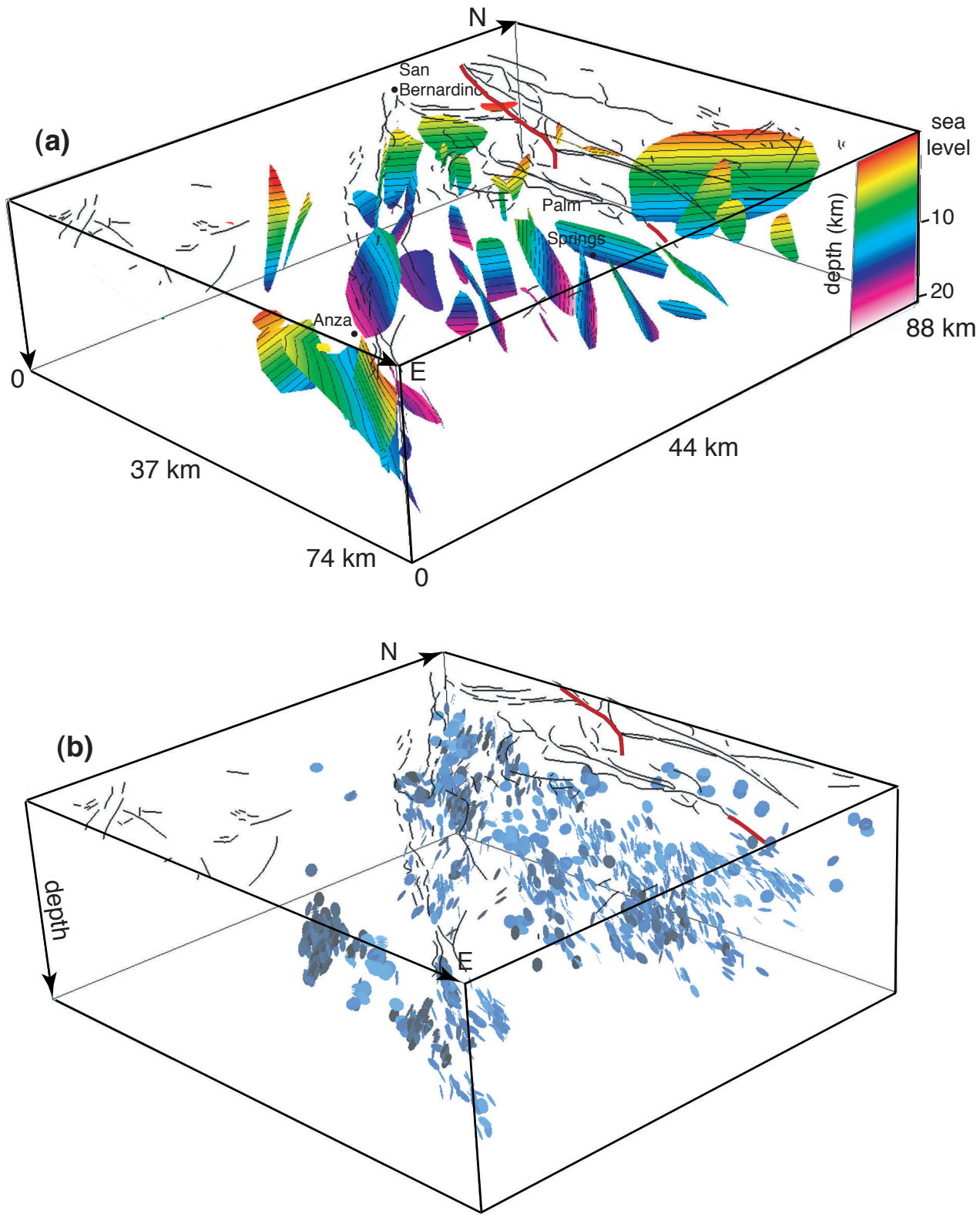

Figure 7. Perspective view of the faults shown in figure 5b (a), and same view of the 1539 nodal planes we have been able to select so far (b).

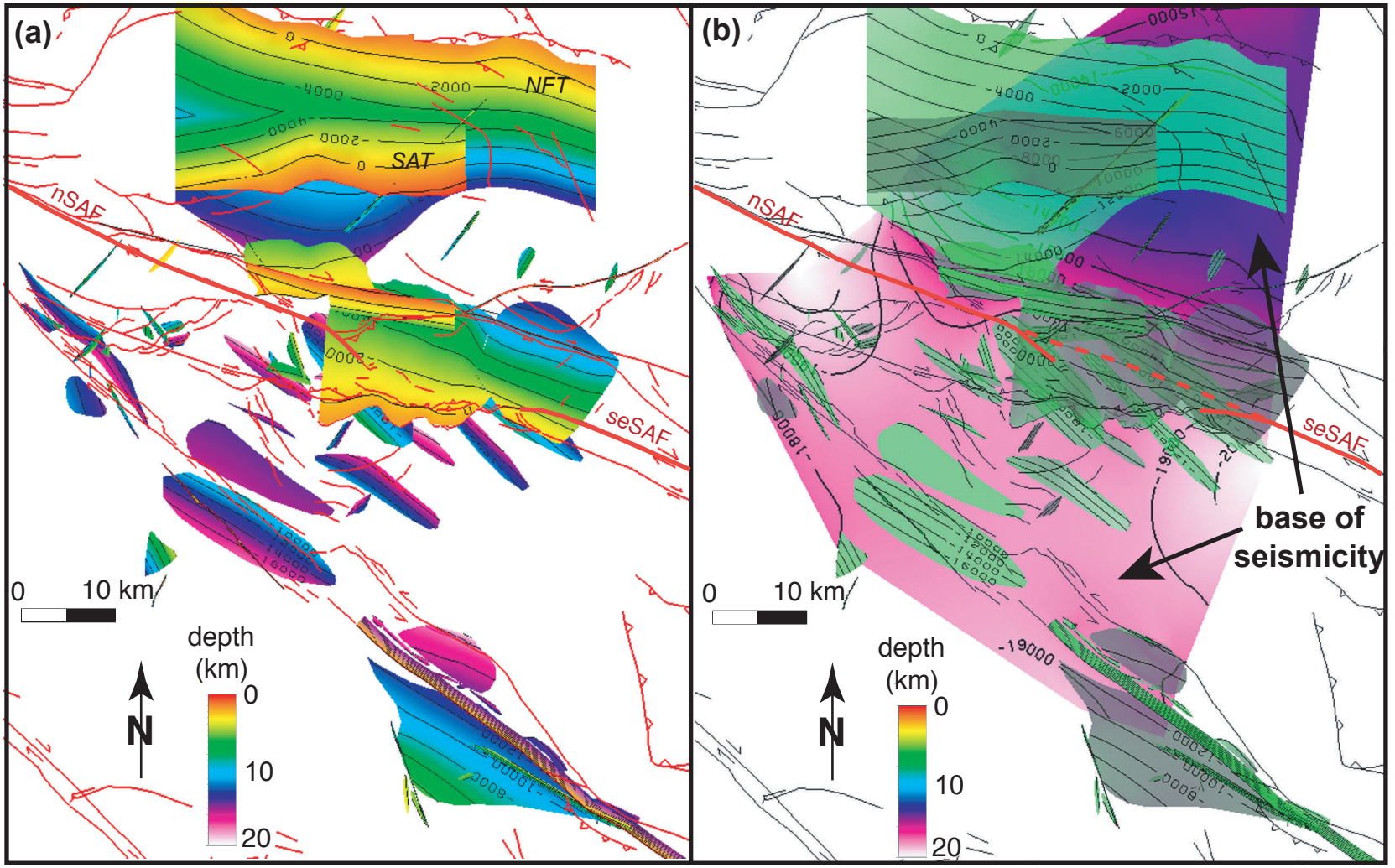

Figure 8. (a) Faults from figure 5b and additional fault models obtained by combining data from published maps and papers . *NFT*=North Frontal thrust, *SAT* = Santa Ana thrust, from *Spotila and Sieh* [2000]. (b) Faults shown together with the surface representing depth of seismicity (shades of pink and blue indicate depth). Depth of earthquakes steps up from 19 km SW of the San Andreas trace to 15 km NE of it. The San Andreas fault trace (the ideal connection between north and south-east termination of the trace is shown as dashed red line) runs parallel to this step. Depth contours in meters b.s.l.

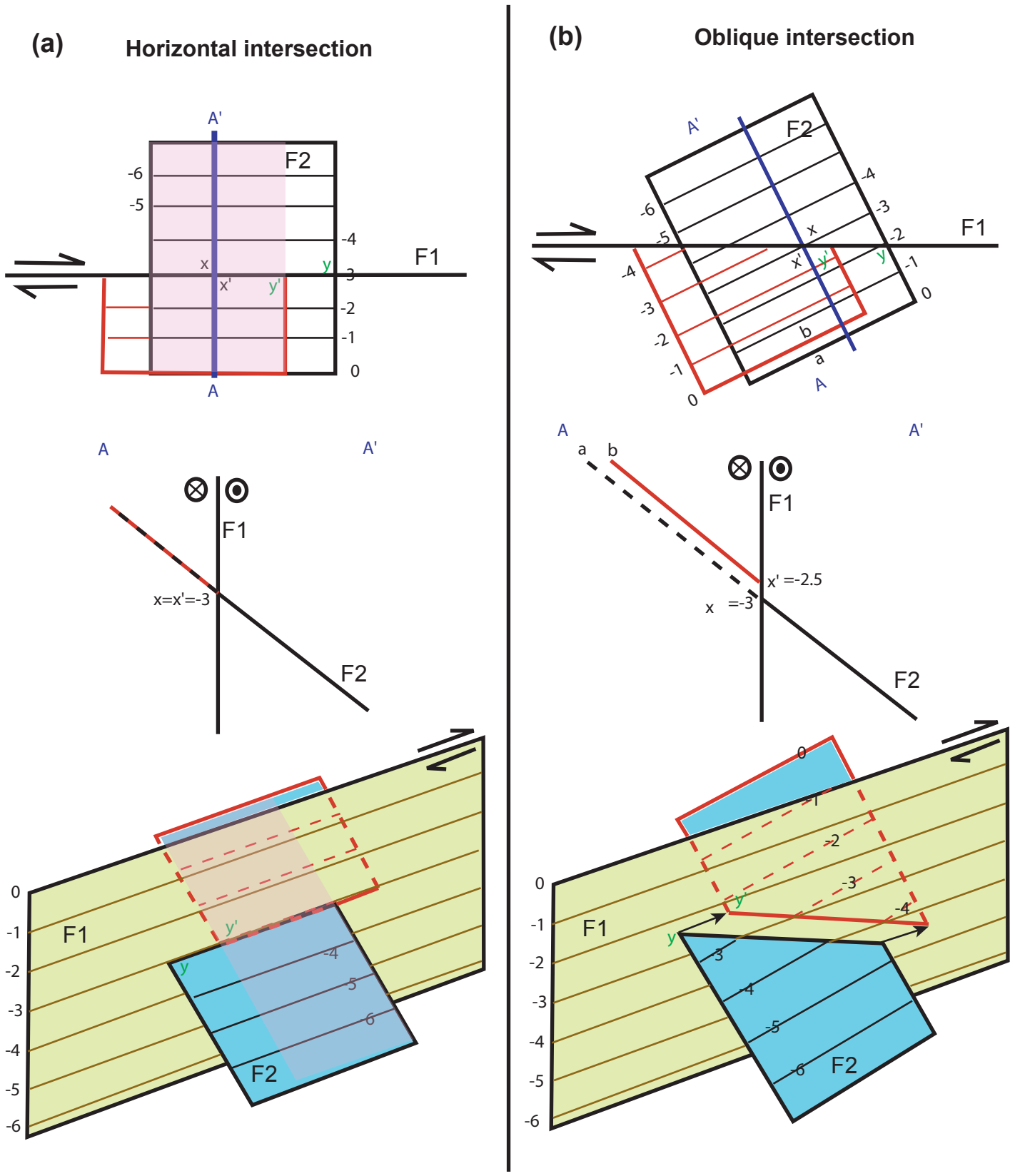

Figure 9. (a) If the intersection between F1 and F2 is horizontal, slip on F1 leaves part of the F2 plane intact (pink area). (b) If the intersection between F1 and F2 is oblique, slip on F1 breaks all continuity of the F2 plane, resulting in likely shut off of F2.

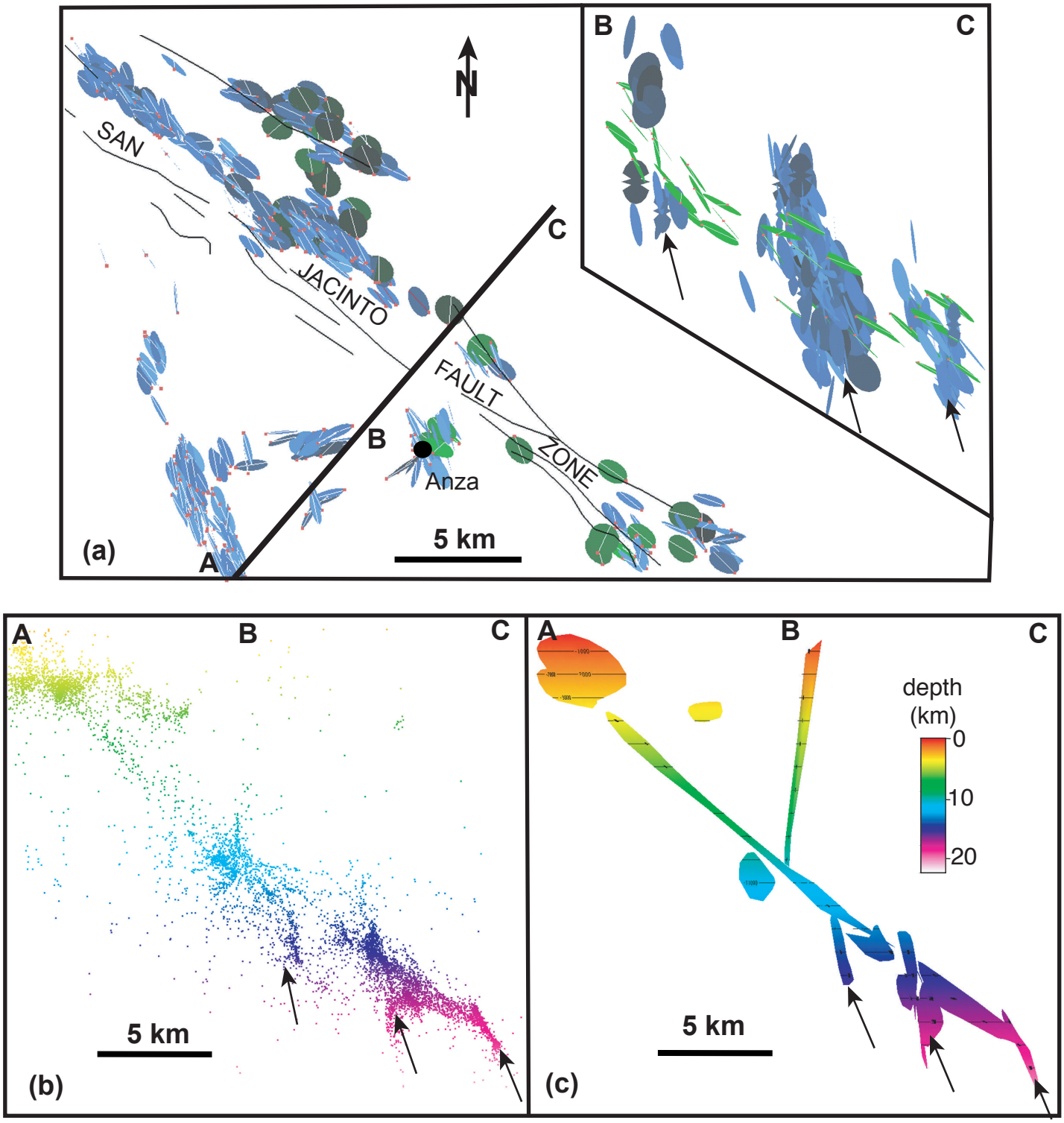

Figure 10. (a) Map of selected nodal planes from the focal mechanisms of *Hauksson* [2000] in the Anza area. Location map in figure 5b. Blue circles=steep faults, green circles=low-angle faults, white line with red dot=slip vector, dot indicates direction of slip of hanging wall (see figure 13). Cross section BC shows 3 groups (black arrows) of steep faults separated by low-angle faults showing a combination of right-lateral and reverse motion. (b), (c) are cross sections showing the hypocenters and the modeled faults respectively, in the same area as the map.

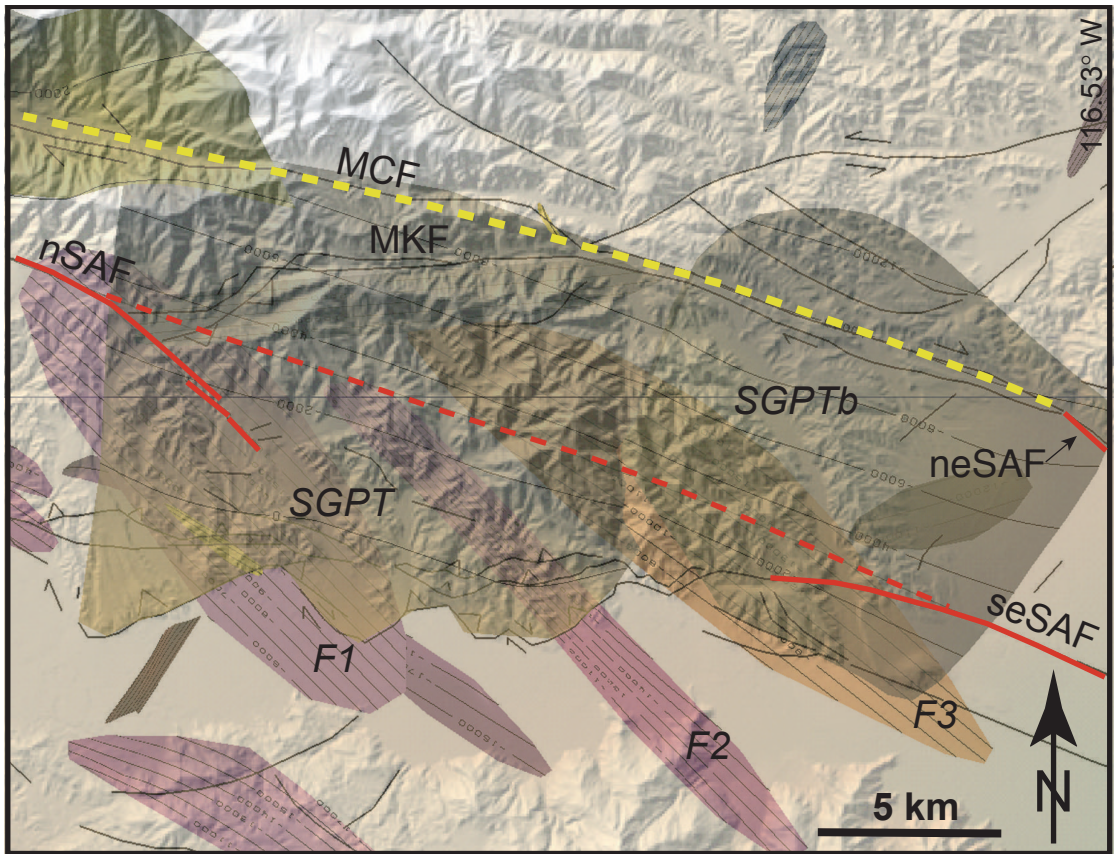

Figure 11. Location of the faults shown in figure 12 with respect to topographic features. SGPT = San Gorgonio Pass thrust, SAF = San Andreas fault. Location map is in figure 1.

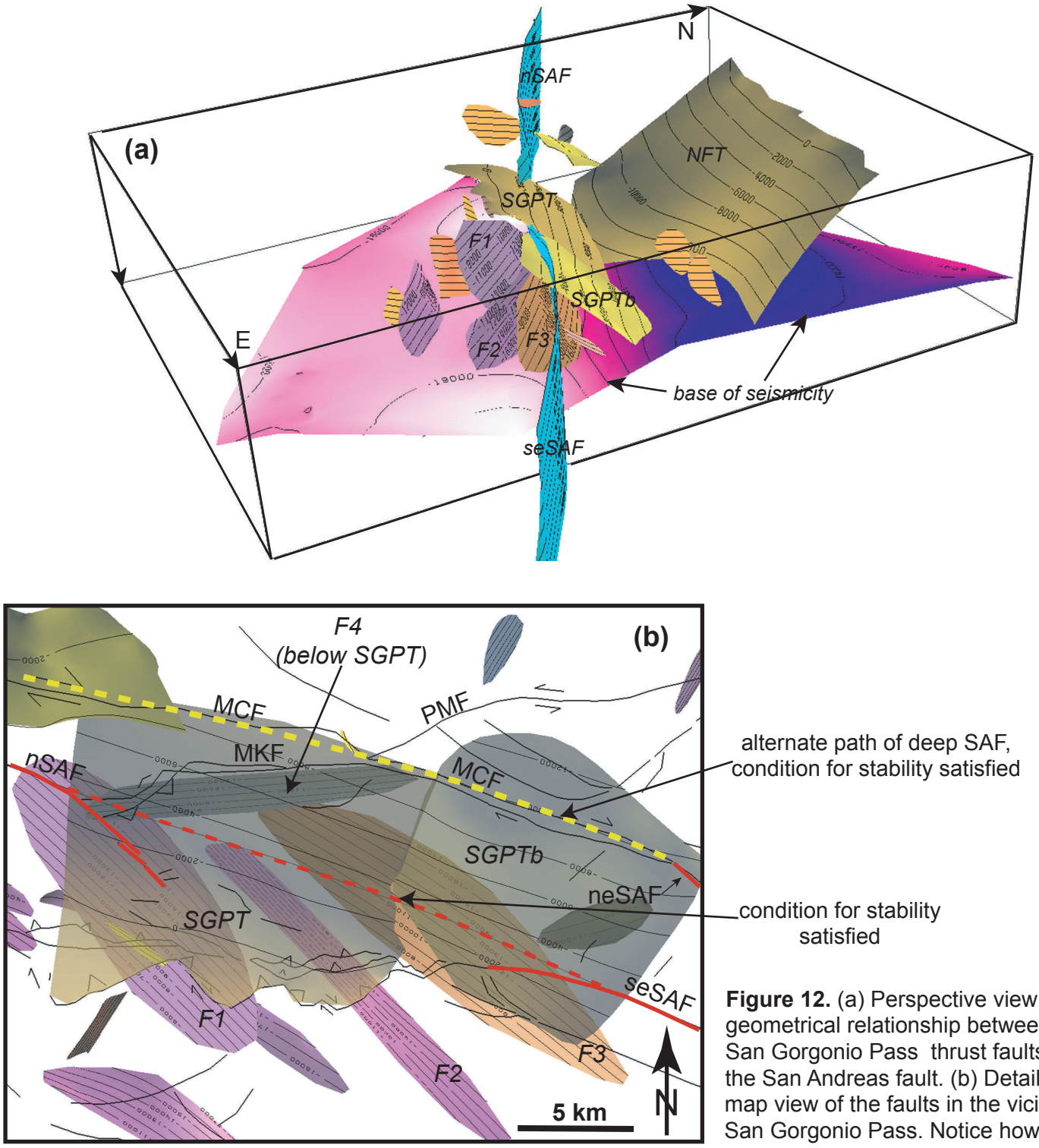

Figure 12. (a) Perspective view of the geometrical relationship between the San Gorgonio Pass thrust faults and the San Andreas fault. (b) Detailed map view of the faults in the vicinity of San Gorgonio Pass. Notice how the simplest connection between nSAF and seSAF (dashed red line) has to cut through fault *F3*. To avoid such intersection, the San Andreas would have to skirt *F3* to the east, possibly following the Mill Creek fault north at depth (dashed yellow line), then turn west to joint the NW San Andreas segment. Any path of the San Andreas south of *F3* would have to be even more complex, or the San Andreas not close to vertical.
SGPT=San Gorgonio Pass thrust; *SGPTb*=section of the San Gorgonio thrust system that ruptured in the 1986 Palm Springs earthquake; SAF=San Andreas fault (*nSAF*=northwestern segment of the San Andreas, *seSAF*=southeastern segment, neSAF=northeastern segment), dashed line indicates simplest possible position of the SAF beneath the SGPT system; NFT=North Frontal thrust [*Spotila and Sieh*, 2000]; MCF=Mill Creek fault; PMF=Pinto Mountain fault. *F1, F2, F3*, *F4* are faults modeled from earthquake data.

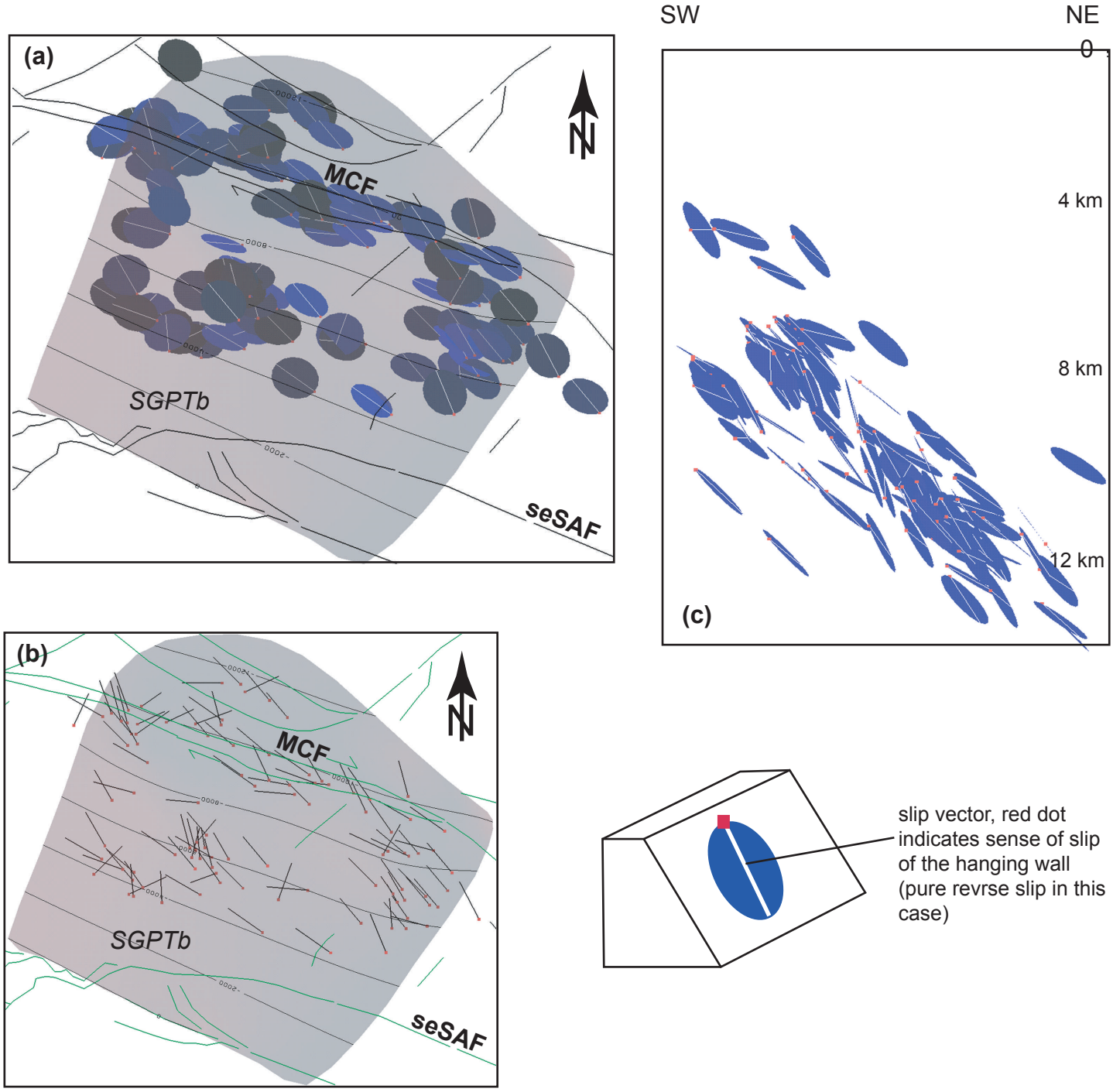

Figure13. (a) Map of the selected nodal planes and slip vectors for the fault that generated the 1986 Palm Springs earthquake (*SGPTb*). (b) same as (a), but only the slip vectors are shown. (c) Cross-section of the nodal planes and slip vectors in (a).

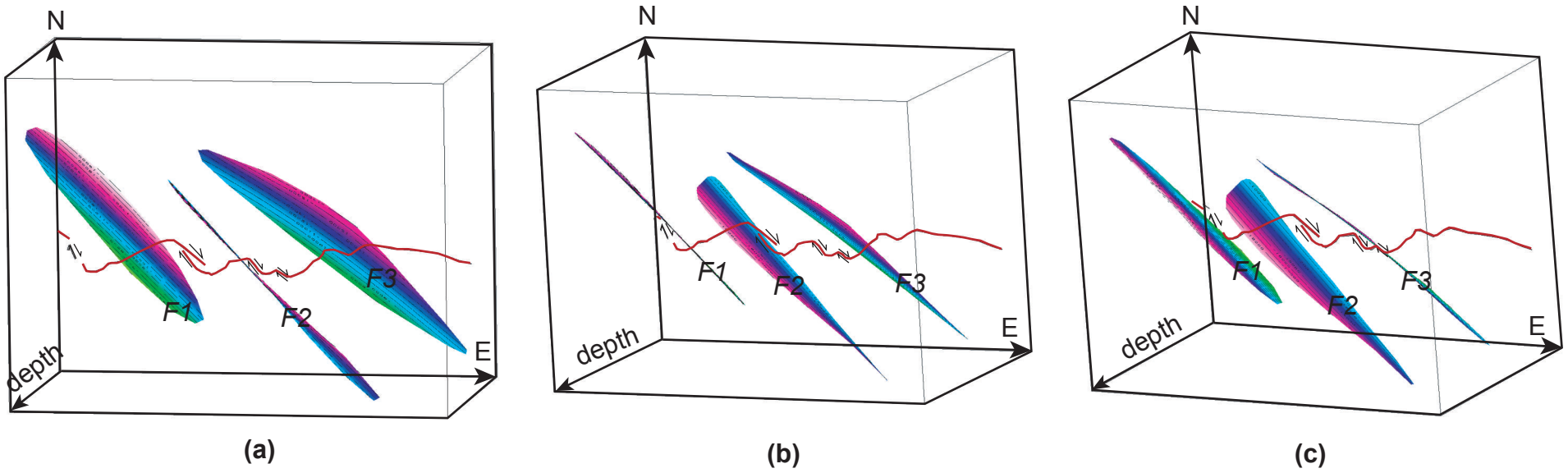

fault depths (m b.s.l.)

	top	bottom
F1	6,000	20,000
F2	10,000	18,000
F3	7,000	17,000

Figure 14. 3D views looking down dip along *F2* (a), *F1* (b), and *F3* (c). The updip projection of each of these three faults falls very close (within 500 m at most) of the right-lateral offsets of the San Gorgonio Pass fault (red trace). Fault depth contours spacing is 1000m. Map views of these faults can be seen in figures 5b, 11, 12b. Focal mechanisms (*Hauksson*, 2000) attributable to these faults consistently show right-lateral and right-lateral/reverse motion.